Chemosphere 331 (2023) 138759

Contents lists available at ScienceDirect

Chemosphere

journal homepage: www.elsevier.com/locate/chemosphere

Magnesium-enriched poultry manure enhances phosphorus bioavailability in biochars

Aline do Amaral Leite [a,b], Leônidas Carrijo Azevedo Melo [a,b], Luis Carlos Colocho Hurtarte [c], Lucia Zuin [d], Cristiano Dela Piccolla [e], Don Werder [f], Itamar Shabtai [g], Johannes Lehmann [b,h,i,*]

[a] Federal University of Lavras/UFLA - Soil Science Dept., 37200-000, Lavras, Brazil
[b] Soil and Crop Sciences, School of Integrative Plant Science, Cornell University, Ithaca, NY, 14850, USA
[c] European Synchrotron Radiation Facility/ESRF – Grenoble, France
[d] Canadian Light Source/CLS – Saskatoon, Canada
[e] University of Western Santa Catarina/UNOESC, Brazil
[f] Cornell Center for Materials Research, Cornell University, Ithaca, NY, 14850, USA
[g] Department of Environmental Science and Forestry, The Connecticut Agricultural. Experiment Station, New Haven, CT, 06511, USA
[h] Department of Global Development, Cornell University, Ithaca, NY, 14850, USA
[i] Cornell Atkinson Center for Sustainability, Cornell University, Ithaca, NY, 14850, USA

HIGHLIGHTS

- Phosphorus bioavailability increases in Mg-enriched biochar up to high pyrolysis temperatures.
- OH^- anions provided with $Mg(OH)_2$ could be a mechanism by which Mg-doped biochars have higher P availability.
- Adding Mg to poultry manure decreased the formation of Ca–P minerals in low temperatures.

GRAPHICAL ABSTRACT

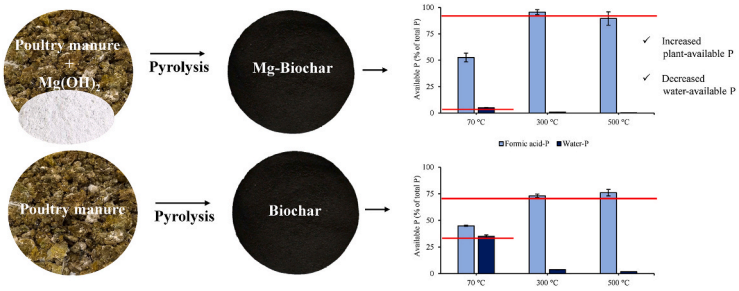

ARTICLE INFO

Handling Editor: X. Cao

Keywords:
Linear combination
P speciation
P extractions
Nutrient recycling

ABSTRACT

Pyrolysis of calcium-rich feedstock (e.g., poultry manure) generates semi-crystalline and crystalline phosphorus (P) species, compromising its short-term availability to plants. However, enriching poultry manure with magnesium (Mg) before pyrolysis may improve the ability of biochar to supply P. This study investigated how increasing the Mg/Ca ratio and pyrolysis temperature of poultry manure affected its P availability and speciation. Mg enrichment by ~2.1% increased P availability (extracted using 2% citric and formic acid) by 20% in Mg-biochar at pyrolysis temperatures up to 600 °C. Linear combination fitting of P K-edge XANES of biochar, and Mg/Ca stoichiometry, indicate that P species, mainly Ca–P and Mg–P, are altered after pyrolysis. At 300 °C, adding Mg as magnesium hydroxide [$Mg(OH)_2$] created $MgNH_4PO_4$ (18%) and $Mg_3(PO_4)_2.8H_2O$ (23%) in the biochar, while without addition of Mg $Ca_3(PO_4)_2$ (11%) predominated, both differing only for pyrophosphate, 33 and 16%, respectively. Similarly, the P $L_{2,3}$ edge XANES data of biochar made with Mg were indicative of either $MgHPO_4.3H_2O$ or $Mg_3(PO_4)_2.8H_2O$, in comparison to $CaHPO_4.2H_2O$ or $Ca_3(PO_4)_2$ without Mg. More importantly, hydroxyapatite [$Ca_5(PO_4)_3(OH)$] was not identified with Mg additions, while it was abundant in biochars

* Corresponding author. Soil and Crop Sciences, School of Integrative Plant Science, Cornell University, Ithaca, NY, 14850, USA.
E-mail address: CL273@cornell.edu (J. Lehmann).

https://doi.org/10.1016/j.chemosphere.2023.138759
Received 20 November 2022; Received in revised form 17 April 2023; Accepted 21 April 2023
Available online 21 April 2023

produced without Mg both at 600 (12%) and 700 °C (32%). The presence of Mg formed Mg–P minerals that could enhance P mobility in soil more than Ca–P, and may have resulted in greater P availability in Mg-enriched biochars. Thus, a relatively low Mg enrichment can be an approach for designing and optimize biochar as a P fertilizer from P-rich excreta, with the potential to improve P availability and contribute to the sustainable use of organic residues.

1. Introduction

Phosphorus (P) is a non-renewable plant nutrient that requires efficient management to ensure its supply for global agriculture. To reduce mining of P resources, adding new P to agroecosystems, and, consequently, polluting the environment and causing P scarcity, acquiring an efficient cycle in agricultural systems is mandatory (Tilman et al., 2001). In tropical soils, P is one of the most limiting nutrients. Therefore, soils receive large amounts of P fertilization with soluble phosphate fertilizers (Roy et al., 2016) to compensate for strong adsorption to iron and aluminum oxides and low-activity clay minerals (Abdala et al., 2012; Lopes and Guimarães Guilherme, 2016; Roy et al., 2016). One proposed solution is to use P from excreta, thereby on the one hand reducing environmental pollution, and on the other hand recycling phosphate fertilizer resources. However, comparatively little information is available on high-performance P fertilizers made from wastes and specifically excreta.

Producing P-rich biochars through pyrolysis may enhance plant P use efficiency in P fixing soils as compared to highly water-soluble P sources (Lustosa Filho et al., 2019). Biochar is a byproduct obtained by thermochemical decomposition of organic feedstocks within a range of pyrolysis temperatures typically between 400 and 800 °C and under low or no oxygen conditions (Ippolito et al., 2015). For woody feedstocks, the resulting carbon-rich product improves soil physical and chemical properties, such as increased soil pH, greater cation exchange capacity, and greater water-holding capacity (Glaser et al., 2002; Ippolito et al., 2015; Joseph et al., 2021). Accordingly, many studies report its use as a soil conditioner rather than as a fertilizer with high agronomic performance (Kumar et al., 2022). Animal-based organic waste is one of the most promising feedstocks for production of biochars and are mainly used for their value as nutrient amendments (Murtaza et al., 2023). These wastes are extensively generated as they are a part of the protein food chain (Akdeniz, 2019), and need to be processed prior to proper land application. Poultry manure is generated in large amounts and is rich in plant nutrients, especially P, with P contents ranging from 1.2 to 1.8% (dry weight basis) (Darby et al., 2016; Suleiman et al., 2018). Its transformation into biochar can be an efficient way to sanitize the manure, while maintaining or even increasing plant availability of P (Carneiro et al., 2018; Rehman et al., 2020). Transforming animal waste into biochar has proven to be an effective method to mitigate environmental contamination not only of pathogens but also of hormones, antibiotics, microplastics, PFAS etc. (Sauvé et al., 2016; Kyakuwaire et al., 2019; Tomul et al., 2020). It is less known whether and under what conditions pyrolysis is also effective in producing a high-efficiency fertilizer (Buss et al., 2020).

The most important parameters controlling the physicochemical and morphological properties of biochars are changes in highest heating temperature and holding time (Enders et al., 2012; Ippolito et al., 2020). The chemical composition of poultry manure is to a large extent dominated by calcium carbonate that is present in poultry diets resulting in a high Ca concentration in manure and consequently a low Mg/Ca ratio (Higashikawa et al., 2010). Its conversion into biochar might form stable Ca–P minerals, and a significant P fraction would become unavailable to plants (Bruun et al., 2017). However, because Mg is a smaller ion than Ca, its incorporation in the manure may cause structural changes, such as destabilization and decomposition of the structure including P species during the heating treatment process (Farzadi et al., 2014; Kannan et al., 2005). A partial substitution of Ca by Mg in synthetic hydroxyapatite production strongly inhibits the crystallinity of phosphates after thermal degradation (Cao and Harris, 2008; Hilger et al., 2020). Little information is available as to the effect of Mg on the water solubility and plant availability of P in biochar made from P-rich excreta or specifically poultry manure.

Therefore, the objectives of this study were (1) to determine how increasing Mg/Ca ratios and highest heating temperature affect biochar-P solubility and crystallinity; (2) to assess changes in P forms in biochar with Mg enrichment, and (3) to elucidate the mechanisms controlling P availability in Mg-enriched biochar and its potential as a fertilizer. We hypothesize that (1) higher ratios of Mg/Ca results in higher P solubility in biochar relevant to plant P uptake; and (2) the addition of Mg decreases the formation of tricalcium phosphate and reduces proportions of crystalline P forms.

2. Materials and methods

2.1. Biomass and pyrolysis conditions

Poultry manure was obtained from the experimental poultry farm at Cornell University collected over the course of several days, using commercial feed containing mostly corn, soybean, wheat, calcium carbonate, salt, choline chloride, yeast extract and mono-dicalcium phosphate [$Ca(H_2PO_4)_2$]. Poultry manure feedstock was oven-dried at 70 °C until constant mass, ground, and sieved (<850 μm) before pyrolysis. All biochars were produced in an adapted laboratory-scale muffle furnace, and the process was performed with a heating rate of 10 °C min^{-1} to their target temperature (300 °C, 500 °C, 600 °C, or 700 °C), with a holding time of 30 min and left to slowly cool down to room temperature. At the end of each cycle, the biochar yield was recorded.

2.2. Feedstock modification

After drying, the poultry manure was pyrolyzed to produce biochar. Before pyrolysis, some of the poultry manure was pre-treated with magnesium hydroxide [$Mg(OH)_2$] to generate Mg-enriched biochar. This source of Mg was selected after tests with other sources (i.e., chloride and sulfate), as it contained no interfering counter-ions (Table S1). Briefly, $Mg(OH)_2$ was mixed with the manure to achieve Mg/Ca ratios of 0.08, 0.10, 0.12, 0.16 and 0.20, soaked in deionized water (1:10, solid-liquid ratio), and stirred with a magnetic ball for 30 min. The mixture was oven-dried at 70 °C (until constant mass) (Zhang et al., 2012).

2.3. Characterization of feedstock and biochars

All samples were crushed with a mortar and pestle and sieved to a thin powder (<250 μm) prior to analyses. Electrical conductivity (EC) and pH were measured in a suspension of 1:20 (w:v) ratio in deionized water, which was first shaken for 90 min on a reciprocal shaker, and measured using a pH and an EC meter (Rajkovich et al., 2012).

Biochars and manure samples were analyzed for total Ca, Mg, and P contents according to Enders and Lehmann (2012). Briefly, 0.20 g of each sample was ashed in a small muffle furnace for 8 h at 500 °C. It was then digested in concentrated nitric acid (70%) at 120 °C, and for the final digestion step, hydrogen peroxide (30%) was added to accelerate the oxidation of organic carbon. Finally, the samples were diluted to a 2% nitric acid (v/v) solution. Contents were filtered, and elements were

measured by inductively coupled plasma spectrometry (ICP, Thermo iCAP 6500 series, Thermo Fisher Scientific, Massachusetts, USA).

Total carbon, hydrogen, oxygen and nitrogen were determined on a Thermo Delta V isotope ratio mass spectrometer (IRMS) interfaced with an NC2500 elemental analyzer. Standards were calibrated against international reference materials provided by the International Atomic Energy Association (IAEA). Ash content from biochars was determined by oven drying (105 °C), and then, heating the samples in open crucibles at 750 °C for 6 h. The BET (Brunauer-Emmett-Teller) surface area (BET – SA, $m^2\ g^{-1}$) and total pore volume (TPV, $cm^3\ kg^{-1}$) data (Table S6) were collected using a Micromeritics 3-Flex gas sorption analyzer. The surface morphological structures, images, and elemental mapping were obtained with high-resolution scanning electron microscopy (MIRA3 FESEM, Tescan, Pennsylvania, USA), equipped with energy-dispersive spectroscopy (EDS), and the EDS spectra collected on a Bruker 6-60 XFlash detector (Bruker, Massachusetts, USA) after mounting samples on a standard SEM stub using carbon tape. The surface functional groups composition was studied using FTIR spectroscopy (Vertex V80V Vacuum FTIR system, Bruker, Massachusetts, USA) in attenuated total reflectance (ATR) mode. The samples were placed in the sample holder and spectra were collected with a spectral range of 4000−600 cm^{-1}, with a resolution of 4 cm^1, averaged over of 64 scans, and processed for baseline correction using OPUS v7.2 (Bruker, Massachusetts, USA).

2.4. Phosphorus extractions

Poultry manure and biochar samples were analyzed for plant-available P using 2% formic acid and 2% citric acid extractions at a ratio of 1:100 (w/v). The samples were shaken with the extractant for 30 min and filtered through qualitative filter paper (Wang et al., 2012). Water-soluble P was extracted by shaking the samples with deionized water for 16 h, at a ratio of 1:150 (w/v), and filtering through qualitative filter paper (Zwetsloot et al., 2015). For all extractions, P concentration was determined using the molybdenum blue method, adapted from Murphy and Riley (1962). Briefly, P concentration in samples was determined by UV–vis spectrophotometry (Shimadzu, Kyoto, Japan) measuring the intensity of the color from the formation of a phospho-molybdic complex (660 nm) produced by the reaction of ammonium molybdate and ascorbic acid according to P concentration in samples.

2.5. Kinetics of P release

Samples of pyrolyzed and unpyrolyzed manure, with and without Mg $(OH)_2$ addition, were selected to determine the kinetics of P release in water. Briefly, samples were mixed with deionized water in a proportion of 1/200 ratio (w/v) and then shaken at 120 rpm for 240 h, and sampled after 0.25, 0.5, 1, 6, 12, 24, 48, 72, 120, and 240 h. The samples were filtered through qualitative filter paper and analyzed for P using the molybdenum blue method (Murphy and Riley, 1962). The P release kinetics was determined by the changes in P concentrations over the sampling time and then fitted to the following models: parabolic diffusion model, Elovich equation, power function, first order, and second-order functions (Carneiro et al., 2021; Liang et al., 2014). The fit of each mathematical model was based on its standard error of the estimative (SE) (Carneiro et al., 2021; Shariatmadari et al., 2006), and the best models were chosen based on the Akaike information criterion (AIC) (Akaike, 1974).

2.6. X-ray absorption near edge spectroscopy (XANES)

The P K-edge XANES analysis was carried out at the IDEAS beamline at the Canadian Light Source (CLS) (Saskatoon, Canada). Fluorescence spectra were collected under vacuum using a Vortex ME4 SDD with FalconX electronics. Samples were loaded in sample holders in the pre-chamber. Information for reference P compounds was obtained from the following sources: magnesium phosphate dibasic ($MgHPO_4.3H_2O$, CAS 7782-75-4, Sigma Aldrich), tricalcium phosphate and calcium phosphate dibasic [$Ca_3(PO_4)_2$ and $CaHPO_4.2H_2O$, respectively (dela Piccolla et al., 2021),], trimagnesium phosphate, struvite, octacalcium phosphate, pyrophosphate, lecithin, hydroxyapatite and phosphate adsorbed on Pahokee peat [$Mg_3(PO_4)_2.8H_2O$, $MgNH_4PO_4$, $Ca_8H_2(PO_4)_6.5H_2O$, P_2O_7, organic-complexed P–Fe, 1200 mmol kg^{-1} of Fe and $Ca_{10}(PO_4)_6(OH)_2$, respectively (Beauchemin et al., 2003; Hesterberg et al., 2017),]. Samples were collected in the energy range of 2085–2245 eV, scanned twice, and checked for reproducibility. The E_0 was set to 2151 eV and energy step sizes were 5 eV from 2085 to 2135 eV, 0.2 eV from 2135 to 2175 eV, 2 eV from 2175 to 2245 eV. The program Athena v0.9.26 (Ravel and Newville, 2005) was used for data processing and analysis of the P K-edge XANES spectra. Data were normalized, pre-edge and post-edge energy regions were set to −65 to −10 eV and 30–60 eV, respectively. Linear combination fitting was performed over the spectral region and above the P adsorption edge (2145–2180 eV). Reported fits were obtained using a modified standard elimination procedure (Hesterberg et al., 2017; Manceau et al., 2012), progressively reducing the number and combinations of standards until reaching a higher accuracy model (coefficients >5% and R factor <0.05). For the final set, a maximum of five standards was allowed for each fit, and an energy shift of up to ±0.5 eV was allowed for the standards individually.

P $L_{2,3}$-edge XANES analyses were carried out at the Variable Line Spacing Plane Grating Monochromator (VLS-PGM) beamline at the Canadian Light Source. The spectra were collected in total fluorescence yield mode (FLY), using a microchannel plate detector and total electron yield (TEY) mode measuring the sample drain current. For normalization purpose, the incident beam current was measured with a Ni mesh located upstream the sample. Scans were performed in triplicates from 130 to 155 eV, with step sizes of 0.1 eV and 1s of dwell time. Merged data were subtracted from a linear background adjusted at an energy level between 130 and 135 eV, followed by extended multiplicative scatter correction and normalization to the peak at 139 eV using Unscrambler X software v10.5.1 (CAMO Software AS, Oslo, Norway). For consistently determining peak positions, peaks were found using Origin Pro v9.90 (Originlab Corp, Massachusetts, USA).

2.7. X-ray diffraction (XRD)

Poultry manure and biochar samples were analyzed by X-ray diffraction analysis (XRD) to detect crystalline phases. Samples were ground, sieved to form a powder suspension, deposited on a SiN3 membrane, and air-dried. The samples were examined by light microscopy to locate regions of interest, consisting of isolated microparticles of biochar. Samples are mounted vertically, perpendicular to the X-ray beam. The energy of the incident beam was chosen around 13.0 keV. The beam was focused to ~2 × 2 μm^2 (flux ~2 × 1012 phs^{-1}, at I = 128 mA electron beam current; attenuated to ~1011 ph s^{-1} by detuning the undulator) using a compound refractive lens set-up (CRL) mounted in a transfocator. X-ray powder diffraction (XRPD) maps were obtained by raster-scanning the samples and collecting 2D XRPD patterns, in transmission, with a Dectris EIGER 4 M single photon counting detector that acquires frames with 2070 × 2167 pixels (75 × 75 μm^2 pixel size) at a rate up to 750 Hz. Azimuthal integration and calculation of crystalline phases by linear fits were performed using dedicated Jupyter Notebooks. For both analytical configurations, the synchrotron diffraction data has been corrected for attenuation effects and processed using the software package PyMCA, region of interest (ROI) imaging was also used to extract averages and statistical analyses (Solé et al., 2007; Fu et al., 2020). Crystalline phases were identified using Match! v2 (Crystal Impact, Bonn, Germany), compared with minerals available at the open crystallography database (COD). The degree of crystallinity was calculated using Origin Pro v9.90 and X'Pert Highscore Plus v3.0.0 (Panalytical, Malvern, UK). The degree of crystallinity of the samples was

defined based on the average crystallite size and degree of crystallinity, considering the calculated areas under the peaks and the width at half-height of the diffraction peak.

3. Data analysis

The extraction of P using citric acid, formic acid, and water was performed in a 5 x 5 factorial design, considering 5 processing temperatures (70 °C, 300 °C, 500 °C, 600 °C, or 700 °C) and 5 Mg/Ca ratios (0.08, 0.10, 0.12, 0.16, and 0.20). The collected data were checked for normality by the Shapiro–Wilk's test prior to other data analyses. When the assumptions for analysis of variance were met (formic acid and citric acid), a linear model was fitted and the significance of the interaction between the factors was tested. Afterwards, the means of the treatments were grouped using the Scott-Knott test ($p \leq 0.05$) to avoid overlapping average results (Scott and Knott, 1974). When the criteria for analysis of variance were not met (water-P), a generalized least squares (GLS) model was used, and if significant, the means of all treatments were compared using the Tukey test ($p \leq 0.05$). Data from the kinetics of P release were fitted to nonlinear models using the *nlstools* package (Baty et al., 2015).

4. Results

4.1. Phosphorus availability

The extractable P portion from unpyrolyzed poultry manure was, on average, 25% lower than in any biochar regardless of Mg/Ca ratio (Fig. 1). Comparing pyrolysis temperatures, at the lowest (300 °C) and highest (700 °C), the range of formic and citric-P was higher than unpyrolyzed biomass, 27 and 23% for biochar (Mg/Ca of 0.08), and 46 and 17% for Mg-biochar (Mg/Ca ratio of 0.16), respectively (Fig. 1 a and b). Across pyrolysis temperatures ranging from 300 to 600 °C, adding Mg resulted in higher P availability (except for a Mg/Ca ratio of 0.2) (Fig. 1 a and b). At 300 °C, citric and formic acid extracted about 16.8 and 16.7 g P kg^{-1} biochar, representing approximately 96 and 94% of the total P when Mg was added. The extractions were significantly lower for biochar without Mg additions, about 14.4 and 13.6 g kg^{-1}, representing about 73 and 70% of total P. With increasing pyrolysis temperature, the effect of $Mg(OH)_2$ addition on extractable P is positive up to 600 °C, with formic-P extractable P of 19.6 g kg^{-1} (90% of total P), and of 15.8 g kg^{-1} (68% of total P) with and without added Mg, respectively. At 700 °C, however, the amounts of formic acid-extractable P were very similar, about 69 and 71% of total P, respectively.

Water-extractable P, however, decreased as a function of pyrolysis temperature and even more as a function of Mg addition (Fig. 1c and Table S2). For unpyrolyzed biomass, at a Mg/Ca ratio of 0.08, water extracted 3.8 g kg^{-1} (35% of total P), and for a Mg/Ca ratio of 0.16, only

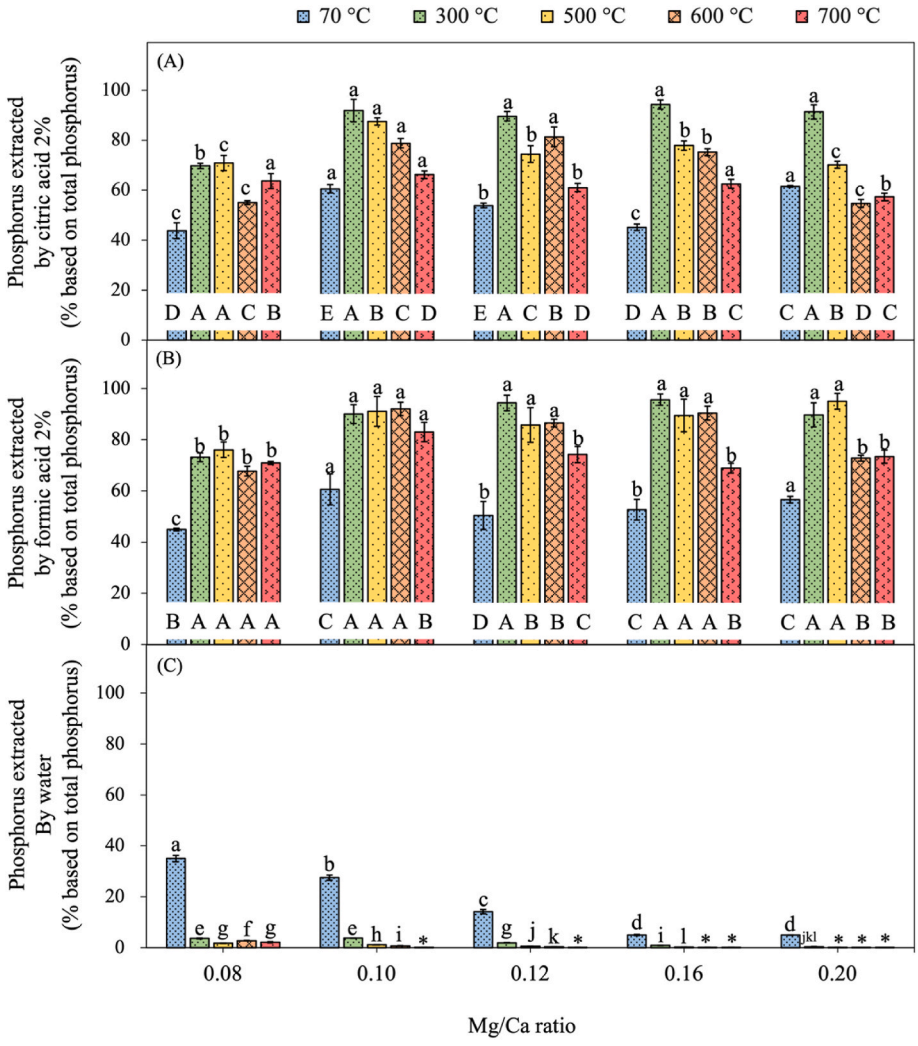

Fig. 1. Phosphorus extracted by citric acid 2% (A), formic acid 2% (B) and water-P (C) as a function of Magnesium hydroxide modified biochars and magnesium and calcium ratios. For citric and formic acids, lowercase letters compare biochars in individual temperature within all Mg/Ca ratios, and uppercase letters compare individual Mg/Ca ratio in all temperatures. The means of the treatments were grouped by the Scott Knot test ($p < 0.05$). For water-P, treatments followed by the same letter do not differ among themselves by the Tukey test ($p < 0.05$). Mean values ± standard deviation; n = 3. The extractable portion in grams per kilogram and percentage are referenced in Table S2. Note: *values lower than 0.0.

0.5 g kg^{-1} (5% of total P). At 300 °C, water-P was even lower for both biochar and Mg-biochar, 0.7 and 0.2 g kg^{-1} (3.7 and 0.9% of total P, respectively).

4.2. Kinetics of phosphorus release

The kinetics of P release from poultry manure pyrolyzed at 300 °C was initially greater than that of unpyrolyzed poultry manure (Fig. 2). However, P release from unpyrolyzed poultry manure did not stabilize at the end of the assay (240 h). Most importantly, Mg additions decreased P release, and more so for pyrolyzed than unpyrolyzed manure. Adding Mg to unpyrolyzed manure decreased P release by 36% of total P, from 5.36 to 3.45 g kg^{-1} in 72 h. At 300 °C, Mg addition had the greatest effect, decreasing P release from 67% to 3% of total P over the entire sampling period. In contrast, biochar and Mg-biochar at 500 °C had a low P release of 4.6 and 1% of total P, respectively (mathematical equations in SI, and fitting parameters in Table S3).

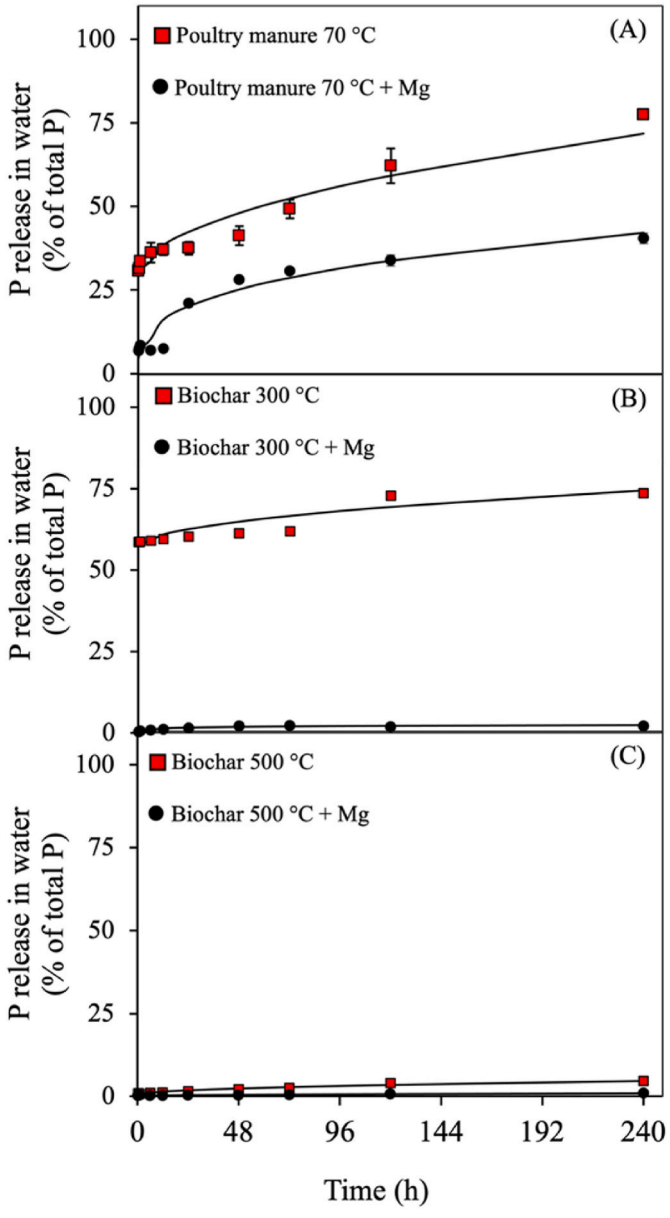

Fig. 2. Kinetics of phosphorus release in water of poultry manure and biochars (Mg/Ca: 0.08) and poultry manure and biochars plus magnesium (Mg/Ca: 0.16). Mean value ± standard deviation, n = 3. Poultry manure and biochars at 70, 300 and 500 °C fitted to parabolic diffusion model; poultry manure and biochars plus magnesium at 70, 300 and 500 °C fitted to power function, Elovich equation and parabolic diffusion model, respectively. Parameters of the examined models are shown in Table S3.

4.3. Phosphorus K and $L_{2,3}$ edge XANES spectroscopy

K edge XANES spectroscopy and the linear combination fitting of P K-edge XANES of biochar and Mg-biochar data indicates that Ca–P and Mg–P species are mainly altered after pyrolysis, with few differences whether or not Mg was added to the unpyrolyzed biomasses (70 °C) (Table 1 and Figs S1, S2 and S3). The P minerals for biomass were $Mg_3(PO_4)_2.8H_2O$ (35.9 and 41.6%), $CaHPO_4.2H_2O$ (16.6 and 23.9%), P–Fe (12.5 and 9.3%), and organic P as lecithin (35.0 and 25.2%) without and with Mg addition, respectively. The Fe–P only appeared for unpyrolyzed biomasses, and lecithin appeared at up to 300 °C only without Mg additions (9.0%). Also, at all pyrolysis temperatures, biochar and Mg-biochar had similar proportions of $CaHPO_4.2H_2O$ and octacalcium phosphate. However, at 300 °C, only Mg-biochar had $MgNH_4PO_4$ (17.9%) and $Mg_3(PO_4)_2.8H_2O$ (23.0%), while biochar without Mg showed $Ca_3(PO_4)_2$ (10.4%), both differing only for pyrophosphate, 32.9 and 16.0%, respectively. Biochars made at temperatures of 500 and 600 °C had similar P compounds but differed whether or not Mg was added. For biochars made at 500 and 600 °C, biochar without Mg showed pyrophosphate (29.8 and 14.0%) and hydroxyapatite (not identified and 12.5%), while Mg-doped biochar showed $Mg_3(PO_4)_2.8H_2O$ (10.4 and 11.2%). At 700 °C, biochar without Mg showed hydroxyapatite (32.5%) and pyrophosphate (15.7%), and Mg-doped biochar showed $Mg_3(PO_4)_2.8H_2O$ (5.2%).

The P $L_{2,3}$ edge XANES data indicate that Mg-biochar presented a shoulder feature at around 139.7–140 eV, which could be either $MgHPO_4.3H_2O$ or $Mg_3(HPO_4).8H_2O$ (Fig. S2 and Table S4). The biochars without Mg addition do not have this Mg–P feature, and even without Mg, they already have a shoulder with a center at 141.7–141.9 eV attributed to $CaHPO_4.2H_2O$ or $Ca_3(PO_4)_2$, more intensely at higher pyrolysis temperatures. These Ca-peaks also appear when Mg is added, but only from 500 °C onwards, with no intense features observed at 300 °C, similar to unpyrolyzed biomass. For all samples, two primary peaks described P features at the energy position at around ~139 and ~147 eV.

4.3.1. Scanning electron microscopy (SEM) and energy dispersive spectroscopy (EDS)

The elemental mapping by SEM revealed a uniform distribution of P and Mg (Fig. 3a) and concentrated Ca spots on the surface of biochars irrespective of Mg additions. Phosphorus is distributed on the surface similarly to Mg. The biochar has a smooth surface with evenly-spread round features, quantified by EDS spectra to have a high concentration of Ca (Table S5). In contrast, features with different spatial patterns were observed in Mg-biochar, such as cubes, flakes, and blocks (Fig. 3b). These patterns have high concentrations of Mg as quantified by EDS (Fig. S4 and Table S5).

4.4. Elemental analysis

Total P concentrations increased in Mg-biochar at high pyrolysis temperatures but decreased at low temperatures (Table 2). For instance, at 300 °C, total P from biochar without Mg addition (Mg/Ca ratio 0.08) decreased from 19.6 to 17.5 g kg^{-1} when Mg was added (Mg/Ca ratio 0.16). In contrast, at 700 °C, total P increased from 23.3 to 25.0 g kg^{-1}, for the same Mg/Ca ratios. Total Mg concentration did not vary substantially as a function of pyrolysis temperature (Table 2). However, on average, the Mg yield was 2-fold higher than its unpyrolyzed biomass for biochar and only 1.3 higher for Mg-biochar.

Table 1
Major phosphorus species determined by linear combination fitting of XANES spectra of standards (Fig. S1) to XANES spectra of biochar of different temperatures with and without magnesium enrichment.

Samples	$MgNH_4PO_4$	$Mg_3(PO_4)_2$	$CaHPO_4$	$Ca_3(PO_4)_2$	OCP	HAP	PYP	P–Fe	Lecithin	R factor
	%									
Poultry manure	–	35.9	16.6	–	–	–	–	12.5	35.0	0.0008
Poultry manure 70 °C + Mg	–	41.6	23.9	–	–	–	–	9.3	25.2	0.0008
Biochar 300 °C	–	–	18.4	10.6	29.2	–	32.9	–	9.0	0.0003
Biochar 300 °C + Mg	17.9	23.0	16.9	–	26.4	–	15.8	–	–	0.0004
Biochar 500 °C	–	–	21.7	8.7	39.7	–	29.8	–	–	0.0007
Biochar 500 °C + Mg	–	10.4	23.8	27.6	38.2	–	–	–	–	0.0005
Biochar 600 °C	–	–	23.7	20.7	28.8	12.5	14.3	–	–	0.0005
Biochar 600 °C + Mg	–	11.2	22.0	26.7	40.0	–	–	–	–	0.0005
Biochar 700 °C	–	–	–	12.2	39.6	32.5	15.7	–	–	0.0004
Biochar 700 °C + Mg	–	5.2	22.9	37.3	34.6	–	–	–	–	0.0007

Note: OCP, Octacalcium phosphate; HAP, Hydroxyapatite; PYP, Pyrophosphate; P–Fe, phosphate adsorbed on Pahokee peat. The spectra of reference P compounds are shown in Fig. S3.

4.5. C, H, N and O contents

The biochars had low C and N contents regardless of their Mg/Ca ratios (Table 2). At 300 °C, the C content of biochar (Mg/Ca ratio 0.16) decreased from 391.7 to 296.7 mg g^{-1} when adding Mg (Mg/Ca ratio 0.16), and at 700 °C, the C content decreased from 313.4 to 155.1 mg g^{-1}. The total N decreased during pyrolysis more than the total C content by the addition of Mg (Mg/Ca ratio of 0.16), from 67.5 to 38.2 mg g^{-1} at 300 °C and from 27.0 to 13.3 mg g^{-1} at 700 °C. The H/C ratio declined as a function of pyrolysis temperature, but no substantial changes were observed as a result of Mg additions. The H/C ratios remained between 0.6 and 0.7 at 300 °C and between 0.2 and 0.3 at 600 °C. In contrast, the O/C ratios varied only as a function of Mg addition, remaining between 0.5 and 0.6, for the Mg/Ca ratios of 0.08 and between 0.8 and 1.2, for Mg/Ca 0.16.

4.6. FTIR spectroscopy

The highest spectral bands intensities in the FTIR spectra were observed between 1625 and 600 cm^{-1} (Fig. 4 and Table S8). With pyrolysis, band intensity decreased at 3190 and 2914 cm^{-1}, assigned to aromatic and aliphatic C–H stretching, respectively, irrespective of Mg addition (Liang et al., 2018; Wang et al., 2014). At 70 °C, $Mg(OH)_2$ addition increased band intensity at 1625 and 1579 cm^{-1}, corresponding to aromatic C═C, and at 1407 cm^{-1}, corresponding to C–O stretching and carbonates (Bekiaris et al., 2016; Domingues et al., 2017; Farah Nadia et al., 2015). At 300 °C, Mg additions increased intensity at 1579 and 1026, corresponding to C═C and P–O or Mg–O bond, and decreased intensity at 873 and 705 cm^{-1}, corresponding to P–*O*–P or P═O stretching (Bekiaris et al., 2016; Li et al., 2016; Nardis et al., 2021). Intensity at 873 cm^{-1} corresponds to Ca–P, and intensity at 1026 cm^{-1} is attributed to P–O bond stretching in Ca–P or Mg–P minerals (Fig. S6). At 500 and 700 °C, Mg additions increased intensity at bands 1407, 1026 and 873 cm^{-1}.

5. Discussion

5.1. Magnesium enrichment increases phosphorus availability on biochar

Phosphorus availability assessed by citric and formic acid extraction increases with Mg addition, up to a pyrolysis temperature of 600 °C (Fig. 1). With pyrolysis, enhanced P availability seems to be consistent with precipitation of Mg minerals determined by P K and $L_{2,3}$-edge [$MgNH_4PO_4$ and $Mg_3(PO_4)_2.8H_2O$] (Table 1 and S4). At the highest examined pyrolysis temperatures (700 °C) Mg–P minerals are reduced. This is consistent with previous studies where Mg–P may gradually decompose as the temperature rises, probably due to instability at high temperatures (Ramlogan and Rouff, 2016). Also, the decomposition of struvite at temperatures higher than 300 °C may explain the decrease in total N in these Mg-biochars, probably due to the evolution of volatiles.

The greater P availability plateaued at a Mg/Ca ratio of 0.10 and even decreases at 0.16, and not only Mg–P minerals were formed in Mg-biochar. As observed by SEM-EDS quantification analysis at 300 °C (Table S5), Mg-biochar has several features (blocks and flakes) of high Mg concentration, which was confirmed by the presence of MgO particles in the form of nano-flakes within the biochar matrix in prior studies (Wu et al., 2019; Zhang et al., 2012), and confirmed by the increase in MgO crystallite size in Mg-biochar in our study (Fig. S5 and Table S7). These Mg-rich spatial features could explain why increasing Mg/Ca ratios do not increase P availability from a certain amount of Mg onwards, as a low or no difference was observed for the highest Mg/Ca ratios to biochar without Mg addition (Fig. 1), thus restricting P and Mg reaction to some extent. Moreover, the success of Mg addition to increase P availability could be influenced by other factors such as P concentration in poultry manure (~11 g P kg^{-1}) and biochar (25 g P kg^{-1}) (Table 2). Therefore, the increase in P availability was affected by the P/Mg ratio. The SEM mapping of P and Mg show both Mg and P evenly distributed on the surface (Fig. 3). This spatial correlation between Mg and P has already been reported for poultry manure at low pyrolysis temperature (300 °C); at high pyrolysis temperatures, however, this correlation decreases in favor of a higher correlation between Ca and P (Bruun et al., 2017).

Phosphorus availability in unpyrolyzed poultry manure was lower compared to that in biochar (Table S2), which could be related to the larger amount of organic P present in manure, e.g., DNA, phytates, and lecithin (Uchimiya and Hiradate, 2014), while biochars usually lack organic P forms as a result of thermal treatment (Zwetsloot et al., 2015). Moreover, as observed by P K-edge XANES analysis, the unpyrolyzed poultry manure had around 35% of organic-complexed lecithin (Table 1). After pyrolysis, organic P decreased as expected, present only at a low proportion at 300 °C (Table 1).

Water-extractable P mainly decreased as a result of pyrolysis and to a minor extent as pyrolysis temperature increased (Table S2), which is explained by the formation of less soluble P minerals after thermal degradation, already at the lowest temperature. Regardless of pyrolysis temperature or indeed because of pyrolyzing at the lowest temperature, it decreased as a function of Mg enrichment. Lower water solubility could have resulted from the OH^- anions provided with $Mg(OH)_2$ additions, and that could also be part of the mechanisms by which Mg-doped biochars have higher P availability assessed by citric and formic acid extractions, since these anions can also react with Ca^{2+} ions, preventing Ca–P precipitation and crystallization with heat treatment.

The kinetics of P release confirms the lower water solubility of P with Mg additions to both pyrolyzed and unpyrolyzed poultry over ten days (Fig. 2), which is in agreement with Mg-enriched biochar (Morais et al., 2023). Most of the P from biochar without Mg is released within ten

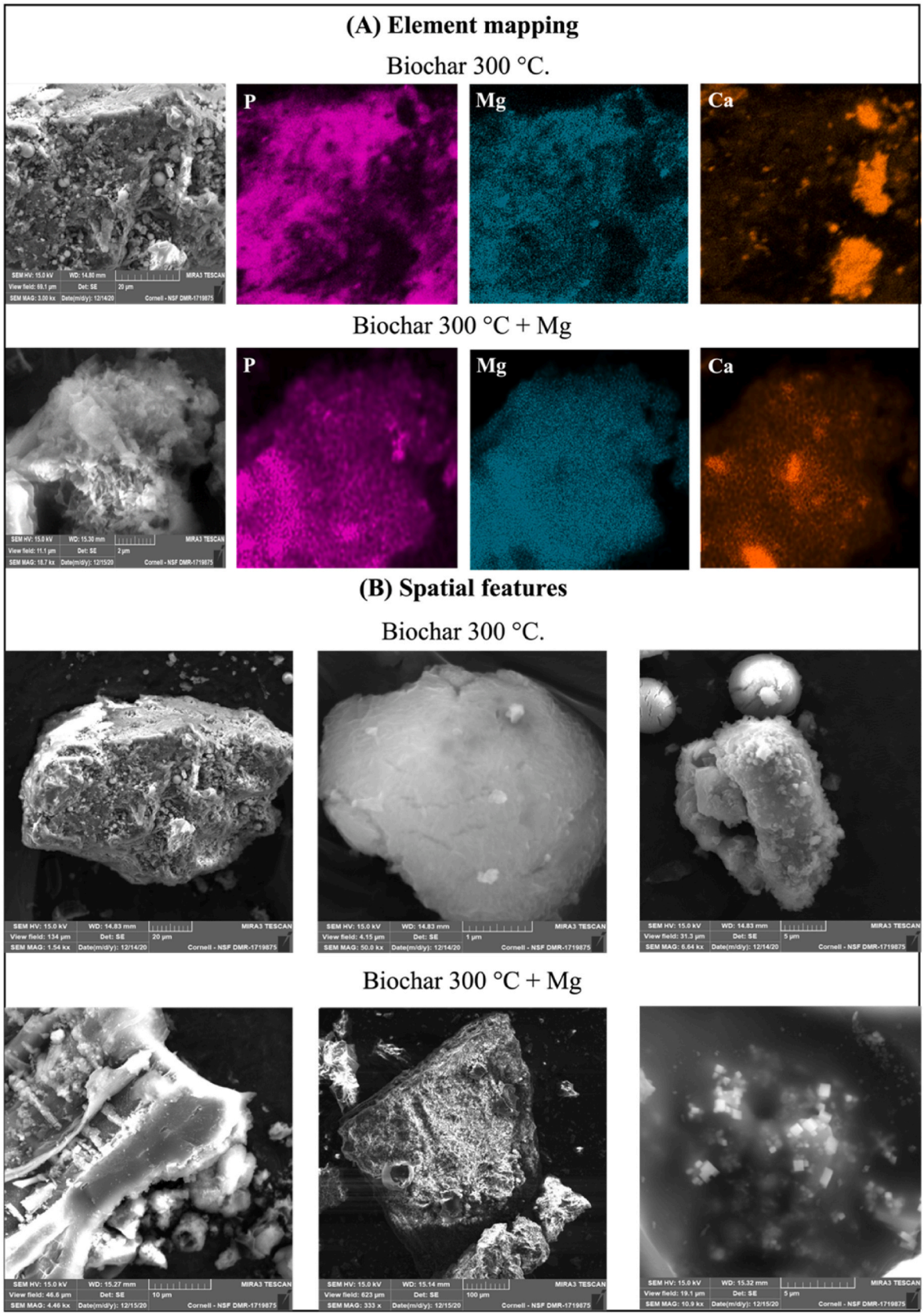

Fig. 3. Scanning electron microscopy (SEM) of biochars with and without Mg additions prior to pyrolysis. (A) Images of biochar pyrolyzed at 300 °C with and without Mg addition (B) Spatial features of biochar pyrolyzed at 300 °C with and without Mg addition. Energy-dispersive spectroscopy (EDS) elemental quantification in Table S5 and Fig. S4.

Table 2
Properties of magnesium hydroxide modified poultry manure and biochar as a function of magnesium and calcium ratios.

Mg/Ca Ratio	T (°C)	pH	EC (ds m^{-1})	Total P (g kg^{-1})	Total Ca (g kg^{-1})	Total Mg (g kg^{-1})	N (mg g^{-1})	C (mg g^{-1})	H (mg g^{-1})	O (mg g^{-1})	H/C (mol mol^{-1})	O/C (mol mol^{-1})	Ash (% w/w)	Biochar Yield (% w/w)
0.08	70	6.5 ± 0.0	4.1 ± 0.1	10.9 ± 0.3	102.7 ± 1.3	6.5 ± 0.1	41.0 ± 0.8	284.5 ± 3.7	45.0 ± 9.0	364.7 ± 12.3	1.9 ± 0.4	1.0 ± 0.0	–	–
	300	10.6 ± 0.1	3.3 ± 0.1	19.6 ± 0.0	164.4 ± 0.4	12.5 ± 0.2	67.5 ± 0.2	391.7 ± 10.7	22.0 ± 2.4	263.0 ± 31.3	0.7 ± 0.1	0.5 ± 0.0	38.2 ± 2.3	57.0 ± 2.7
	500	11.3 ± 0.1	3.7 ± 0.1	21.4 ± 0.5	173.4 ± 6.0	13.2 ± 0.3	33.8 ± 0.2	335.4 ± 2.4	8.5 ± 0.1	264.8 ± 1.0	0.3 ± 0.0	0.6 ± 0.0	47.7 ± 3.1	50.3 ± 5.8
	600	11.7 ± 0.0	4.1 ± 0.2	23.1 ± 2.6	169.1 ± 0.6	13.3 ± 0.1	25.5 ± 0.2	296.5 ± 8.0	6.3 ± 0.7	253.0 ± 1.5	0.3 ± 0.0	0.6 ± 0.0	47.3 ± 0.5	48.7 ± 0.6
	700	11.9 ± 0.0	4.8 ± 0.1	23.3 ± 0.8	178.5 ± 0.9	13.5 ± 0.4	27.0 ± 1.2	313.4 ± 12.3	3.6 ± 0.7	226.1 ± 19.2	0.1 ± 0.0	0.5 ± 0.1	49.0 ± 1.5	47.0 ± 1.0
0.10	70	6.4 ± 0.1	4.4 ± 0.1	11.1 ± 0.4	103.9 ± 3.9	9.9 ± 0.0	60.7 ± 6.1	330.0 ± 32.4	40.8 ± 4.7	360.7 ± 20.5	1.5 ± 0.0	0.8 ± 0.0	–	–
	300	11.5 ± 0.0	5.6 ± 0.1	20.1 ± 0.2	167.5 ± 1.3	15.1 ± 0.1	43.5 ± 9.3	301.8 ± 43.6	13.7 ± 0.1	266.3 ± 1.0	0.6 ± 0.1	0.7 ± 0.1	42.4 ± 2.3	56.7 ± 0.6
	500	11.2 ± 0.1	5.8 ± 0.0	23.5 ± 0.9	171.8 ± 2.9	16.8 ± 0.1	30.4 ± 0.0	317.0 ± 6.1	7.5 ± 0.1	247.6 ± 2.7	0.3 ± 0.0	0.6 ± 0.0	53.5 ± 1.8	50.0 ± 2.0
	600	12.4 ± 0.1	7.2 ± 0.0	25.1 ± 0.6	180.8 ± 4.0	17.2 ± 0.3	21.9 ± 2.9	243.4 ± 15.8	4.4 ± 0.1	260.6 ± 6.8	0.2 ± 0.0	0.8 ± 0.0	54.6 ± 1.4	47.0 ± 1.0
	700	12.6 ± 0.0	8.4 ± 0.0	27.3 ± 0.1	195.5 ± 0.2	18.4 ± 0.3	27.0 ± 4.4	257.7 ± 31.5	3.8 ± 0.1	246.3 ± 4.4	0.2 ± 0.0	0.7 ± 0.1	59.3 ± 1.7	41.7 ± 0.6
0.12	70	9.0 ± 0.0	4.9 ± 0.0	10.9 ± 0.3	109.5 ± 2.5	13.2 ± 0.1	33.4 ± 3.5	266.3 ± 20.6	37.2 ± 1.9	352.9 ± 3.8	1.7 ± 0.2	1.0 ± 0.1	–	–
	300	9.8 ± 0.3	3.1 ± 0.2	19.5 ± 0.6	166.2 ± 2.5	19.2 ± 0.1	38.8 ± 4.7	300.5 ± 22.0	13.7 ± 0.6	275.9 ± 4.2	0.6 ± 0.1	0.7 ± 0.0	45.6 ± 1.7.	60.0 ± 2.0
	500	11.3 ± 0.1	4.6 ± 0.3	24.2 ± 0.1	176.8 ± 1.3	21.3 ± 0.1	15.9 ± 2.0	239.2 ± 12.7	6.6 ± 0.4	246.3 ± 6.0	0.3 ± 0.0	0.8 ± 0.1	57.4 ± 0.6	51.3 ± 1.5
	600	11.5 ± 0.1	5.6 ± 0.3	22.4 ± 0.7	189.7 ± 6.0	20.7 ± 0.6	14.2 ± 0.7	248.0 ± 13.2	4.8 ± 0.7	259.7 ± 2.6	0.2 ± 0.0	0.8 ± 0.0	53.7 ± 1.1	48.0 ± 3.5
	700	12.0 ± 0.0	5.5 ± 0.1	25.9 ± 0.5	180.0 ± 2.3	23.7 ± 0.3	22.7 ± 1.0	250.0 ± 3.7	4.1 ± 0.4	258.1 ± 1.7	0.2 ± 0.0	0.8 ± 0.0	53.4 ± 0.8	49.3 ± 0.6
0.16	70	9.3 ± 0.0	5.7 ± 0.2	11.2 ± 0.1	106.1 ± 0.4	20.8 ± 0.1	45.3 ± 4.0	309.2 ± 18.9	38.0 ± 0.5	366.5 ± 4.7	1.5 ± 0.1	0.9 ± 0.0	–	–
	300	11.1 ± 0.0	4.5 ± 0.2	17.5 ± 0.6	158.5 ± 4.5	25.5 ± 0.3	38.2 ± 0.9	296.7 ± 7.5	17.6 ± 2.8	302.9 ± 9.6	0.7 ± 0.1	0.8 ± 0.0	45.6 ± 1.0	58.7 ± 2.5
	500	12.1 ± 0.0	6.1 ± 0.2	21.9 ± 0.1	178.0 ± 1.3	27.5 ± 0.0	17.5 ± 0.5	231.9 ± 3.3	5.0 ± 0.1	271.6 ± 5.7	0.3 ± 0.0	0.9 ± 0.0	50.2 ± 0.6	50.3 ± 0.6
	600	12.0 ± 0.0	5.5 ± 0.2	21.4 ± 0.5	170.4 ± 5.3	27.1 ± 0.5	21.5 ± 1.5	272.7 ± 11.8	5.8 ± 0.4	264.2 ± 1.8	0.3 ± 0.0	0.7 ± 0.0	56.6 ± 0.2	50.3 ± 1.5
	700	12.2 ± 0.0	7.4 ± 0.1	25.0 ± 0.1	206.1 ± 0.1	28.5 ± 0.0	13.3 ± 0.3	155.1 ± 1.7	3.3 ± 1.0	244.4 ± 7.5	0.3 ± 0.1	1.2 ± 0.0	64.5 ± 3.0	46.0 ± 2.7
0.20	70	10.1 ± 0.0	6.1 ± 0.0	8.7 ± 0.2	79.2 ± 7.4	28.6 ± 0.2	47.5 ± 2.0	246.0 ± 3.1	39.0 ± 1.9	364.9 ± 3.8	1.9 ± 0.1	1.1 ± 0.0	–	–
	300	11.3 ± 0.0	4.8 ± 0.0	16.9 ± 0.3	126.1 ± 0.7	29.4 ± 0.0	33.8 ± 3.1	223.2 ± 1.4	15.8 ± 0.7	263.0 ± 13.9	0.8 ± 0.0	0.9 ± 0.0	56.7 ± 1.0	59.7 ± 2.5
	500	12.1 ± 0.1	4.9 ± 0.0	17.8 ± 0.3	149.7 ± 3.6	29.5 ± 0.0	10.4 ± 0.1	161.4 ± 4.2	4.9 ± 0.3	216.7 ± 0.4	0.4 ± 0.0	1.0 ± 0.0	64.9 ± 1.5	50.3 ± 1.1
	600	12.2 ± 0.1	5.3 ± 0.2	19.3 ± 1.3	154.8 ± 1.6	29.5 ± 0.1	9.3 ± 1.1	137.7 ± 5.1	3.3 ± 0.2	207.3 ± 3.5	0.3 ± 0.0	1.1 ± 0.1	68.2 ± 0.3	48.3 ± 1.1
	700	12.4 ± 0.0	6.4 ± 0.0	20.4 ± 0.2	163.8 ± 1.9	29.5 ± 0.0	11.6 ± 0.2	126.1 ± 0.7	2.5 ± 0.3	188.7 + 3.1	0.2 ± 0.0	1.1 ± 0.0	746 ± 1.7	45.0 ± 1.0

Mean values ± standard deviation; (pH, EC, Ash, Biochar yield, n = 3; Total Ca, P, Mg, N, C, H and O, n = 2).

days, getting close to what is determined to be plant available using citric and formic acid extraction (Fig. 2). In comparison, Mg-doped biochar and Mg-doped unpyrolyzed manure had a lower P release rate even after ten days. However, the lower P availability in water does not correlate with P fertilizer potential from these sources, as plants may improve P dissolution and absorption through several mechanisms (Morgan and Connolly, 2013), primarily through rhizosphere acidification. Besides, P sources with low water-soluble P are less susceptible to strong adsorption to soil minerals and, therefore, might have a sustained P release over the plant growth cycle (Hart et al., 2004), which is desirable in tropical soils due to its high P adsorption capacity.

5.2. *Magnesium enrichment decreases the formation of highly crystalline calcium phosphates*

Adding Mg to poultry manure biomass prevented or decreased the formation of Ca–P minerals (Table 1). As suggested by P K-edge XANES analysis, Mg-doped biochar has lower proportions of pyrophosphate (low temperature) and no detectable hydroxyapatite (high temperature), a highly crystalline P compound (Table 1). Previous studies have reported that the partial substitution of Ca by Mg (a smaller ion) inhibits the crystallinity of synthetic hydroxyapatite via inhibiting crystal growth propagation during thermal degradation (Cao and Harris, 2008; Hilger et al., 2020). Thus, the data from this study confirms that this also happens in manure biochar, and it may be the main mechanism involved in the greater P availability.

Besides being a smaller ion and causing structural changes, Mg has a larger hydrated ionic radius than Ca, a reason why Mg–P minerals could enhance P mobility in soil more than Ca–P. An increase in P solubility in calcareous soil due to an increase in Mg/Ca ratios on the exchange complex has already been reported (Manimel Wadu et al., 2013), making the enrichment of manure and its biochar with Mg a promising approach also for high-pH soils. However, further studies on Mg/Ca ratios on P availability are still necessary for both acidic and alkaline

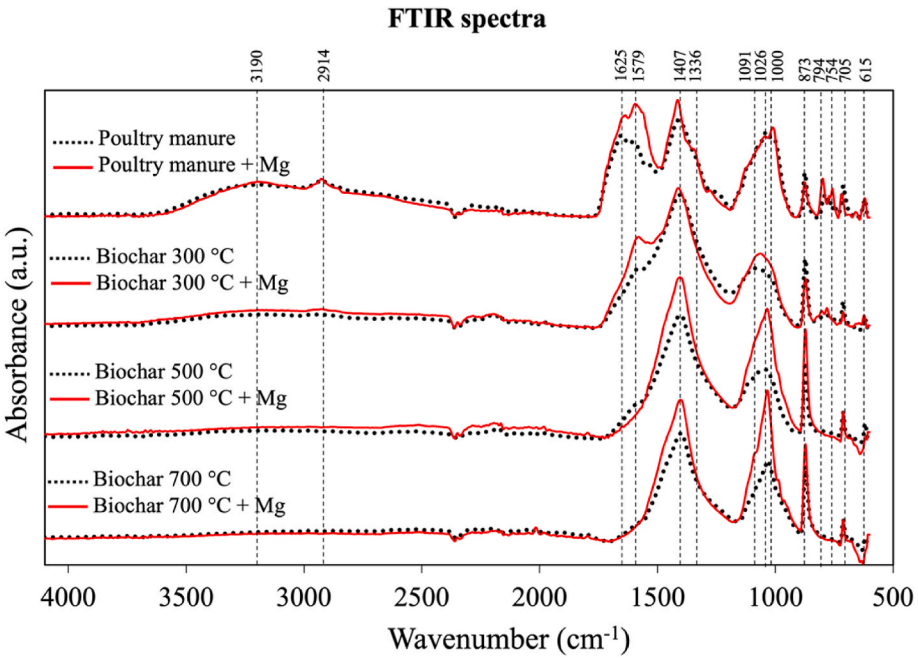

Fig. 4. FTIR spectra and spectral bands of unmodified (Mg/Ca: 0.08) and Mg added (Mg/Ca: 0.16) poultry manure and biochars. FTIR peaks assignments in Table S8.

soils.

Besides forming Mg–P minerals, adding Mg did not entirely prevent P from binding to Ca, as we still observed increasing proportions of $CaHPO_4.2H_2O$, $Ca_3(PO_4)_2$, and octacalcium phosphate (Table 1) with increasing pyrolysis temperatures. High Ca concentrations can result from poultry diets. At the highest examined pyrolysis temperature of 700 °C, the proportions of $CaHPO_4.2H_2O$ and $Ca_3(PO_4)_2$ decrease in favor of hydroxyapatite formation (Table 1), a process that does not occur with Mg additions. For Mg-doped biochar, the abundance of $CaHPO_4.2H_2O$ as shown by decreasing intensity of the FTIR band 873 cm^{-1} at 300 °C (Fig. 4). At the same temperature, the intensity of the band at 1026 cm^{-1} decreased, which could either be $Ca_3(PO_4)_2$ or $Mg_3(PO_4)_2$ minerals, as they have similar features (Fig. S6). However, no features for $Ca_3(PO_4)_2$ were observed for Mg-doped biochar at 300 °C in the K and $L_{2,3}$-edge XANES spectra, and the band at 1026 cm^{-1} is therefore likely caused by $Mg_3(PO_4)_2$. Thus, Mg–P precipitation at low pyrolysis temperatures may have been responsible for preventing hydroxyapatite formation at higher temperatures.

At 500 and 700 °C, however, Mg-biochar had increased band intensities at both 1026 and 873 cm^{-1} (Fig. 4 and Table S8), consistent with increases in Ca–P or Mg–P compounds, likely to be P–Ca compounds as determined by P K and $L_{2,3}$-edge XANES. This indicated that pyrolyzing at temperatures above 700 °C would probably no longer have a positive effect of Mg on P availability or crystallinity.

Regarding the abundance of minerals without P, calcite is observed, which is consistent with this type of material (Domingues et al., 2017). The presence of cristobalite (SiO_2) and periclase (MgO) (Fig. S5) was also observed in studies with poultry litter biochar (Domingues et al., 2017; Lustosa Filho et al., 2017; Yuan et al., 2011). The increase in crystallite size of MgO is compatible with a Mg enrichment (Fig. S5 and Table S7). In response to the thermal treatment, the degree of crystallinity of biochar was higher than in the original manure, indicating a decrease in its amorphous and aliphatic structure, consequently increasing its aromaticity, resulting in a higher-order material with lower reactivity (Lu et al., 2002; Xie et al., 2019). However, no significant changes were observed in the general degree of crystallinity in biochar with or without Mg addition, except for higher crystallinity observed for MgO (Fig. S5 and Table S7).

6. Conclusion

The enrichment of poultry manure biomass with magnesium hydroxide for biochar production increased phosphorus availability through the increase of Mg–P compounds at lower pyrolysis temperature and consequently less proportions of hydroxyapatite at higher pyrolysis temperature. The resulting low water solubility of P can reduce losses and improve the efficiency of Mg-doped manure and Mg-doped biochar to supply P to plants, improving management for this and other Ca-rich manure (e.g., pig manure or dairy manure). For biochar, pyrolysis of Mg-enriched manure biomass can reduce the volume required for application, and the higher P availability can increase the efficiency of phosphate fertilization, decreasing the need for completely soluble P fertilizer in doses higher than plant requirement. For future research, it is necessary to study the effects of microbial solubilization and subsequent plant uptake from Mg-enriched biochar.

Credit author statement

Conceptualization: AdAL, LCAM, JL. Methodology: AdAL, LCAM, JL. Laboratory Analysis: AdAL. Validation: AdAL, LCAM, JL. Investigation: AdAL, LCAM, JL. Formal analysis: All authors. Visualization: All authors. Writing - original draft: AdAL. Resources: JL. Supervision: LCAM, JL. Project administration LCAM, JL. Funding acquisition: JL Writing - review & editing: All authors.

Declaration of competing interest

The authors declare that they have no known competing financial interests or personal relationships that could have appeared to influence the work reported in this paper.

Data availability

Data will be made available on request.

Acknowledgments

This work was funded in part by USDA-NIFA (2019-67021-29945),

USDA-Hatch (2018-19-204). The first author received a scholarship from the Improvement of Higher Education Personnel (CAPES - Proex 88887.358193/2019–00, and CAPES - PrInt 88887.465631/2019–00). The XRD experiments were performed on beamline ID13 at the European Synchrotron Radiation Facility (ESRF), Grenoble, France. We are grateful to Manfred Burghammer for providing assistance in beamline ID13. Part of the research described in this paper was performed through the MAPLE project, a collaboration between the Canadian Light Source (CLS) and the Brazilian Synchrotron Light Laboratory (LNLS-CNPEM). Canadian Light Source, a national research facility of the University of Saskatchewan is supported by the Canada Foundation for Innovation (CFI), the Natural Sciences and Engineering Research Council (NSERC), the National Research Council (NRC), the Canadian Institutes of Health Research (CIHR), the Government of Saskatchewan, and the University of Saskatchewan. The Brazilian Synchrotron Light Laboratory, part of the Brazilian Center for Research in Energy and Materials (CNPEM), is a private non-profit organization under the supervision of the Brazilian Ministry for Science, Technology, and Innovations (MCTI). The authors thank Dr D. Muir for the support at the IDEAS beamline. The authors thank Dr Dean Hesterberg for the support with P K-edge XANES analysis and phosphate standards. This work also made use of the Cornell Center for Materials Research Facilities supported by the National Science Foundation under Award Number DMR-1719875. We thank the Department of Chemistry & Chemical Biology at Cornell and Mary Zick for BET (Brunauer-Emmett-Teller) surface area and total pore volume analysis. We thank Shannan Sweet, Ivan Ribeiro, Annette Dathe, Jefferson Carneiro, Barbara Nardis and Akio Enders, for help with sample analyses.

Appendix A. Supplementary data

Supplementary data to this article can be found online at https://doi.org/10.1016/j.chemosphere.2023.138759.

References

Abdala, D.B., Ghosh, A.K., da Silva, I.R., de Novais, R.F., Alvarez Venegas, V.H., 2012. Phosphorus saturation of a tropical soil and related P leaching caused by poultry litter addition. Agric. Ecosyst. Environ. 162, 15–23. https://doi.org/10.1016/j.agee.2012.08.004.

Akaike, H., 1974. A new look at the statistical model identification. IEEE Trans. Automat. Control 19, 716–723. https://doi.org/10.1109/TAC.1974.1100705.

Akdeniz, N., 2019. A systematic review of biochar use in animal waste composting. Waste Manag. 88, 291-300. https://doi.org/10.1016/j.wasman.2019.03.054.

Baty, F., Ritz, C., Charles, S., Brutsche, M., Flandrois, J.-P., Delignette-Muller, M.-L., 2015. A Toolbox for Nonlinear Regression in R: the Package Nlstools. Journal of Statistical Software 66, 1–12. https://doi.org/10.18637/jss.v066.i05.

Beauchemin, S., Hesterberg, D., Chou, J., Beauchemin, M., Simard, R.R., Sayers, D.E., 2003. Speciation of phosphorus in phosphorus-enriched agricultural soils using X-ray absorption near-edge structure spectroscopy and chemical fractionation. J. Environ. Qual. 32, 1809–1819. https://doi.org/10.2134/jeq2003.1809.

Bekiaris, G., Peltre, C., Jensen, L.S., Bruun, S., 2016. Using FTIR-photoacoustic spectroscopy for phosphorus speciation analysis of biochars. Spectrochim. Acta Mol. Biomol. Spectrosc. 168, 29–36. https://doi.org/10.1016/j.saa.2016.05.049.

Bruun, S., Harmer, S.L., Bekiaris, G., Christel, W., Zuin, L., Hu, Y., Jensen, L.S., Lombi, E., 2017. The effect of different pyrolysis temperatures on the speciation and availability in soil of P in biochar produced from the solid fraction of manure. Chemosphere 169, 377–386. https://doi.org/10.1016/j.chemosphere.2016.11.058.

Buss, W., Bogush, A., Ignatyev, K., Mašek, O., 2020. Unlocking the fertilizer potential of waste-derived biochar. ACS Sustain. Chem. Eng. 8, 12295–12303. https://doi.org/10.1021/acssuschemeng.0c04336.

Cao, X., Harris, W., 2008. Carbonate and magnesium interactive effect on calcium phosphate precipitation. Environ. Sci. Technol. 42, 436–442. https://doi.org/10.1021/es0716709.

Carneiro, J.S. da S., Ribeiro, I.C.A., Nardis, B.O., Barbosa, C.F., Lustosa Filho, J.F., Melo, L.C.A., 2021. Long-term effect of biochar-based fertilizers application in tropical soil: agronomic efficiency and phosphorus availability. Sci. Total Environ. 760 https://doi.org/10.1016/j.scitotenv.2020.143955.

Carneiro, J.S.D.S., Lustosa Filho, J.F., Nardis, B.O., Ribeiro-Soares, J., Zinn, Y.L., Melo, L.C.A., 2018. Carbon stability of engineered biochar-based phosphate fertilizers. ACS Sustain. Chem. Eng. 6, 14203–14212. https://doi.org/10.1021/acssuschemeng.8b02841.

Darby, I., Xu, C.Y., Wallace, H.M., Joseph, S., Pace, B., Bai, S.H., 2016. Short-term dynamics of carbon and nitrogen using compost, compost-biochar mixture and organo-mineral biochar. Environ. Sci. Pollut. Control Ser. 23, 11267–11278. https://doi.org/10.1007/s11356-016-6336-7.

dela Piccolla, C., Hesterberg, D., Muraoka, T., Novotny, E.H., 2021. Optimizing pyrolysis conditions for recycling pig bones into phosphate fertilizer. Waste Manag. 131, 249–257. https://doi.org/10.1016/j.wasman.2021.06.012.

Domingues, R.R., Trugilho, P.F., Silva, C.A., de Melo, I.C.N.A., Melo, L.C.A., Magriotis, Z. M., Sánchez-Monedero, M.A., 2017. Properties of biochar derived from wood and high-nutrient biomasses with the aim of agronomic and environmental benefits. PLoS One 12, e0176884. https://doi.org/10.1371/journal.pone.0176884.

Enders, A., Hanley, K., Whitman, T., Joseph, S., Lehmann, J., 2012. Characterization of biochars to evaluate recalcitrance and agronomic performance. Bioresour. Technol. 114, 644–653. https://doi.org/10.1016/j.biortech.2012.03.022.

Enders, A., Lehmann, J., 2012. Comparison of wet-digestion and dry-ashing methods for total elemental analysis of biochar. Commun. Soil Sci. Plant Anal. 43, 1042–1052. https://doi.org/10.1080/00103624.2012.656167.

Farah Nadia, O., Xiang, L.Y., Lie, L.Y., Chairil Anuar, D., Mohd Afandi, M.P., Azhari Baharuddin, S., 2015. Investigation of physico-chemical properties and microbial community during poultry manure co-composting process. J. Environ. Sci. (China) 28, 81–94. https://doi.org/10.1016/j.jes.2014.07.023.

Farzadi, A., Bakhshi, F., Solati-Hashjin, M., Asadi-Eydivand, M., Osman, N.A.A., 2014. Magnesium incorporated hydroxyapatite: synthesis and structural properties characterization. Ceram. Int. 40, 6021–6029. https://doi.org/10.1016/j.ceramint.2013.11.051.

Fu, C.-C., Tran, H.N., Chen, X.-H., Juang, R.-S., 2020. Preparation of polyaminated Fe3O4@chitosan core-shell magnetic nanoparticles for efficient adsorption of phosphate in aqueous solutions. J. Ind. Eng. Chem. 83, 235–246. https://doi.org/10.1016/j.jiec.2019.11.033.

Glaser, B., Lehmann, J., Zech, W., 2002. Ameliorating physical and chemical properties of highly weathered soils in the tropics with charcoal - a review. Biol. Fertil. 35, 219–230. https://doi.org/10.1007/s00374-002-0466-4.

Hart, M.R., Quin, B.F., Nguyen, M.L., 2004. Phosphorus runoff from agricultural land and direct fertilizer effects: a review. J. Environ. Qual. 33, 1954–1972. https://doi.org/10.2134/jeq2004.1954.

Hesterberg, D., McNulty, I., Thieme, J., 2017. Speciation of soil phosphorus assessed by XANES spectroscopy at different spatial scales. J. Environ. Qual. 46, 1190–1197. https://doi.org/10.2134/jeq2016.11.0431.

Higashikawa, F.S., Silva, C.A., Bettiol, W., 2010. Chemical and physical properties of organic residues. Rev Bras Cienc Solo 34, 1743–1752. https://doi.org/10.1590/s0100-06832010000500026.

Hilger, D.M., Hamilton, J.G., Peak, D., 2020. The influences of magnesium upon calcium phosphate mineral formation and structure as monitored by x-ray and vibrational spectroscopy. Soil Syst 4, 8. https://doi.org/10.3390/soilsystems4010008.

Ippolito, J.A., Cui, L., Kammann, C., Wrage-Mönnig, N., Estavillo, J.M., Fuertes-Mendizabal, T., Cayuela, M.L., Sigua, G., Novak, J., Spokas, K., Borchard, N., 2020. Feedstock choice, pyrolysis temperature and type influence biochar characteristics: a comprehensive meta-data analysis review. Biochar2 421–438. https://doi.org/10.1007/s42773-020-00067-x.

Ippolito, J.A., Spokas, K.A., Novak, J.M., Lentz, R.D., Cantrell, K.B., 2015. Biochar elemental composition and factors influencing nutrient retention. In: Lehmann, J., Joseph, S. (Eds.), for Environmental Management: Science, Technology and Implementation. Routledge, London, pp. 139–163.

Joseph, S., Cowie, A.L., van Zwieten, L., Bolan, N., Budai, A., Buss, W., Cayuela, M.L., Graber, E.R., Ippolito, J.A., Kuzyakov, Y., Luo, Y., Ok, Y.S., Palansooriya, K.N., Shepherd, J., Stephens, S., Weng, Z., Lehmann, J., 2021. How biochar works, and when it doesn't: a review of mechanisms controlling soil and plant responses to biochar. Global Change Biol. Bioenergy 13, 1731-1764. https://doi.org/10.1111/gcbb.12885.

Kannan, S., Lemos, I.A.F., Rocha, J.H.G., Ferreira, J.M.F., 2005. Synthesis and characterization of magnesium substituted biphasic mixtures of controlled hydroxyapatite/β-tricalcium phosphate ratios. J. Solid State Chem. 178, 3190–3196. https://doi.org/10.1016/j.jssc.2005.08.003.

Kumar, A., Bhattacharya, T., Mukherjee, S., Sarkar, B., 2022. A perspective on biochar for repairing damages in the soil–plant system caused by climate change-driven extreme weather events. Biochar 4, 22. https://doi.org/10.1007/s42773-022-00148-z.

Kyakuwaire, M., Olupot, G., Amoding, A., Nkedi-Kizza, P., Basamba, T.A., 2019. How safe is chicken litter for land application as an organic fertilizer? A review. Int. J. Environ. Res. Publ. Health 16, 3521. https://doi.org/10.3390/ijerph16193521.

Li, R., Wang, J.J., Zhou, B., Awasthi, M.K., Ali, A., Zhang, Z., Lahori, A.H., Mahar, A., 2016. Recovery of phosphate from aqueous solution by magnesium oxide decorated magnetic biochar and its potential as phosphate-based fertilizer substitute. Bioresour. Technol. 215, 209–214. https://doi.org/10.1016/j.biortech.2016.02.125.

Liang, X., Jin, Y., He, M., Niyungeko, C., Zhang, J., Liu, C., Tian, G., Arai, Y., 2018. Phosphorus speciation and release kinetics of swine manure biochar under various pyrolysis temperatures. Environ. Sci. Pollut. Control Ser. 25, 25780–25788. https://doi.org/10.1007/s11356-017-0640-8.

Liang, Y., Cao, X., Zhao, L., Xu, X., Harris, W., 2014. Phosphorus release from dairy manure, the manure-derived biochar, and their amended soil: effects of phosphorus nature and soil property. J. Environ. Qual. 43, 1504–1509. https://doi.org/10.2134/jeq2014.01.0021.

Lopes, A.S., Guimarães Guilherme, L.R., 2016. A career perspective on soil management in the Cerrado region of Brazil. In: Advances in Agronomy. Academic Press Inc., pp. 1–72. https://doi.org/10.1016/bs.agron.2015.12.004

Lu, L., Kong, C., Sahajwalla, V., Harris, D., 2002. Char structural ordering during pyrolysis and combustion and its influence on char reactivity. Fuel 81, 1215–1225. https://doi.org/10.1016/S0016-2361(02)00035-2.

Lustosa Filho, J.F., Barbosa, C.F., Carneiro, J.S. da, S., Melo, L.C.A., 2019. Diffusion and phosphorus solubility of biochar-based fertilizer: visualization, chemical assessment and availability to plants. Soil Tillage Res. 194, 104298 https://doi.org/10.1016/j.still.2019.104298.

Lustosa Filho, J.F., Penido, E.S., Castro, P.P., Silva, C.A., Melo, L.C.A., 2017. Co-pyrolysis of poultry litter and phosphate and magnesium generates alternative slow-release fertilizer suitable for tropical soils. ACS Sustain. Chem. Eng. 5, 9043–9052. https://doi.org/10.1021/acssuschemeng.7b01935.

Manceau, A., Marcus, M.A., Grangeon, S., 2012. Determination of Mn valence states in mixed-valent manganates by XANES spectroscopy. Am. Mineral. 97, 816–827. https://doi.org/10.2138/am.2012.3903.

Manimel Wadu, M.C.W., Michaelis, V.K., Kroeker, S., Akinremi, O.O., 2013. Exchangeable calcium/magnesium ratio affects phosphorus behavior in calcareous soils. Soil Sci. Soc. Am. J. 77, 2004–2013. https://doi.org/10.2136/sssaj2012.0102.

Morais, E.G. de, Jindo, K., Silva, C.A., 2023. Biochar-based phosphate fertilizers: synthesis, properties, kinetics of P release and recommendation for crops grown in Oxisols. Agronomy 13, 326. doi:10.3390/agronomy13020326.

Morgan, J.B., Connolly, E.L., 2013. Plant-soil interactions: nutrient uptake. Nature Education Knowledge 4, 2.

Murphy, J., Riley, J.P., 1962. A modified single solution method for the determination of phosphate in natural waters. Anal. Chim. Acta 27, 31–36. https://doi.org/10.1016/S0003-2670(00)88444-5.

Murtaza, G., Ahmed, Z., Eldin, S.M., Ali, B., Bawazeer, S., Usman, M., Iqbal, R., Neupane, D., Ullah, A., Khan, A., Hassan, M.U., Ali, I., Tariq, A., 2023. Biochar-Soil-Plant interactions: a cross talk for sustainable agriculture under changing climate. Front. Environ. 11, 1059449. https://doi.org/10.3389/fenvs.2023.1059449.

Nardis, B.O., Santana Da Silva Carneiro, J., Souza, I.M.G. de, Barros, R.G. de, Azevedo Melo, L.C., 2021. Phosphorus recovery using magnesium-enriched biochar and its potential use as fertilizer. Arch. Agron Soil Sci. 67, 1017–1033. https://doi.org/10.1080/03650340.2020.1771699.

Rajkovich, S., Enders, A., Hanley, K., Hyland, C., Zimmerman, A.R., Lehmann, J., 2012. Corn growth and nitrogen nutrition after additions of biochars with varying properties to a temperate soil. Biol. Fertil. Soils 48, 271–284. https://doi.org/10.1007/s00374-011-0624-7.

Ramlogan, M.v., Rouff, A.A., 2016. An investigation of the thermal behavior of magnesium ammonium phosphate hexahydrate. J. Therm. Anal. Calorim. 123, 145–152. https://doi.org/10.1007/s10973-015-4860-1.

Ravel, B., Newville, M., 2005. ATHENA, artemis, hephaestus: data analysis for X-ray absorption spectroscopy using IFEFFIT. In: J. Synchrotron Rad. 12,, pp. 537–541. https://doi.org/10.1107/S0909049505012719.

Rehman, A., Nawaz, S., Alghamdi, H.A., Alrumman, S., Yan, W., Nawaz, M.Z., 2020. Effects of manure-based biochar on uptake of nutrients and water holding capacity of different types of soils. Case Studies in Chemical and Environmental Engineering 2, 100036. https://doi.org/10.1016/j.cscee.2020.100036.

Roy, E.D., Richards, P.D., Martinelli, L.A., Coletta, L. della, Lins, S.R.M., Vazquez, F.F., Willig, E., Spera, S.A., VanWey, L.K., Porder, S., 2016. The phosphorus cost of agricultural intensification in the tropics. Nature Plants 2, 16043. https://doi.org/10.1038/NPLANTS.2016.43.

Sauvé, S., Bernard, S., Sloan, P., 2016. Environmental sciences, sustainable development and circular economy: alternative concepts for trans-disciplinary research. Environ. Dev. 17, 48–56. https://doi.org/10.1016/j.envdev.2015.09.002.

Scott, A.J., Knott, M., 1974. A cluster analysis method for grouping means in the analysis of variance. Biometrics 30, 507–512. https://doi.org/10.2307/2529204.

Shariatmadari, H., Shirvani, M., Jafari, A., 2006. Phosphorus release kinetics and availability in calcareous soils of selected arid and semiarid toposequences. Geoderma 132, 261–272. https://doi.org/10.1016/j.geoderma.2005.05.011.

Solé, V.A., Papillon, E., Cotte, M., Walter, P., Susini, J., 2007. A multiplatform code for the analysis of energy-dispersive X-ray fluorescence spectra. Spectrochim. Acta Part B At. Spectrosc. 62, 63–68. https://doi.org/10.1016/j.sab.2006.12.002.

Suleiman, A.K.A., Lourenço, K.S., Pitombo, L.M., Mendes, L.W., Roesch, L.F.W., Pijl, A., Carmo, J.B., Cantarella, H., Kuramae, E.E., 2018. Recycling organic residues in agriculture impacts soil-borne microbial community structure, function and N2O emissions. Sci. Total Environ. 631 (632), 1089–1099. https://doi.org/10.1016/j.scitotenv.2018.03.116.

Tilman, D., Fargione, J., Wolff, B., D'Antonio, C., Dobson, A., Howarth, R., Schindler, D., Schlesinger, W.H., Simberloff, D., Swackhamer, D., 2001. Forecasting agriculturally driven global environmental change. Science 292, 281–284.. https://doi.org/10.1126/science.1057544.

Tomul, F., Arslan, Y., Kabak, B., Trak, D., Kendüzler, E., Lima, E.C., Tran, H.N., 2020. Peanut shells-derived biochars prepared from different carbonization processes: comparison of characterization and mechanism of naproxen adsorption in water. Sci. Total Environ. 726, 137828 https://doi.org/10.1016/j.scitotenv.2020.137828.

Uchimiya, M., Hiradate, S., 2014. Pyrolysis temperature-dependent changes in dissolved phosphorus speciation of plant and manure biochars. J. Agric. Food Chem. 62, 1802–1809. https://doi.org/10.1021/jf4053385.

Wang, T., Camps-Arbestain, M., Hedley, M., Bishop, P., 2012. Predicting phosphorus bioavailability from high-ash biochars. Plant Soil 357, 173–187. https://doi.org/10.1007/s11104-012-1131-9.

Wang, Y., Yin, R., Liu, R., 2014. Characterization of biochar from fast pyrolysis and its effect on chemical properties of the tea garden soil. J. Anal. Appl. Pyrolysis 110, 375–381. https://doi.org/10.1016/j.jaap.2014.10.006.

Wu, L., Wei, C., Zhang, S., Wang, Y., Kuzyakov, Y., Ding, X., 2019. MgO-modified biochar increases phosphate retention and rice yields in saline-alkaline soil. J. Clean. Prod. 235, 901–909. https://doi.org/10.1016/j.jclepro.2019.07.043.

Xie, Y., Yang, H., Zeng, K., Zhu, Y., Hu, J., Mao, Q., Liu, Q., Chen, H., 2019. Study on CO2 gasification of biochar in molten salts: reactivity and structure evolution. Fuel 254,115614. https://doi.org/10.1016/j.fuel.2019.06.022.

Yuan, J.H., Xu, R.K., Zhang, H., 2011. The forms of alkalis in the biochar produced from crop residues at different temperatures. Bioresour. Technol. 102, 3488–3497. https://doi.org/10.1016/j.biortech.2010.11.018.

Zhang, M., Gao, B., Yao, Y., Xue, Y., Inyang, M., 2012. Synthesis of porous MgO-biochar nanocomposites for removal of phosphate and nitrate from aqueous solutions. Chem. Eng. J. 210, 26–32. https://doi.org/10.1016/j.cej.2012.08.052.

Zwetsloot, M.J., Lehmann, J., Solomon, D., 2015. Recycling slaughterhouse waste into fertilizer: how do pyrolysis temperature and biomass additions affect phosphorus availability and chemistry? J. Sci. Food Agric. 95, 281–288. https://doi.org/10.1002/jsfa.6716.